

**STUDIES ON GRAPHITIC CARBON NITRIDE
NANOSTRUCTURES FOR PHOTOVOLTAIC APPLICATIONS**

SAURABH PAREEK



**DEPARTMENT OF ENERGY SCIENCE AND ENGINEERING
INDIAN INSTITUTE OF TECHNOLOGY DELHI**

April 2023

©Indian Institute of Technology Delhi (IITD), New Delhi, 2023

**STUDIES ON GRAPHITIC CARBON NITRIDE
NANOSTRUCTURES FOR PHOTOVOLTAIC APPLICATIONS**

by

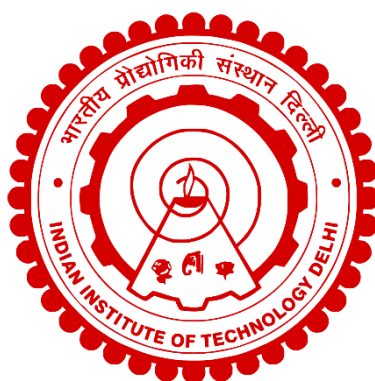
SAURABH PAREEK

Department of Energy Science and Engineering

Submitted

In fulfilment of the requirements of the degree of Doctor of Philosophy

to the



INDIAN INSTITUTE OF TECHNOLOGY DELHI

APRIL 2023

*Dedicated to
My Parents...*

CERTIFICATE

This is to certify that the thesis entitled, “**Studies on graphitic carbon nitride nanostructures for photovoltaic applications**”, submitted by **Mr. Saurabh Pareek** to the Department of Energy Science and Engineering, Indian Institute of Technology Delhi, for the award of the degree of the **Doctor of Philosophy** is a record bonafide research work carried out by him under my supervision and guidance. The results contained in this thesis have not been submitted in part or full, to any other University or Institute for the award of any degree/diploma.

Date:

Dr. Supravat Karak

Place: New Delhi.

Department of Energy Science and Engineering

Indian Institute of Technology Delhi

Hauz Khas, New Delhi-110016, India

Acknowledgments

First and foremost, I want to offer my praise and gratitude to **God Almighty**, for the blessings, peace, strength, and health, He bestowed upon me to finish my research work.

The Doctor of Philosophy is not just a degree but a journey. Today when I am about to reach the destination, I realized that pursuing a Ph.D. requires a lot of hard work, and patience and is somewhat a lonely path. This thesis has become a reality with the kind support and help of many individuals. I would like to extend my sincere gratitude to all of them.

In this regard, firstly I am thankful to my dissertation advisor, **Dr. Supravat Karak** (Associate Professor, DESE), under his guidance I learned the basics of my research work. I am highly indebted for his support and guidance in carrying out my research work and formulating the work into a publishable story. I admire and appreciate his valuable suggestions and insights throughout my Ph.D. work. His prompt inspiration, timely suggestions with kindness, enthusiasm, and dynamism have enabled me to complete this thesis.

I would also like to thank **Prof. K A Subramanyam**, Head of the Department of Energy Science and Engineering (DESE) for his support during my Ph.D. I express my gratitude to the members of my Ph.D. research committee, **Prof. Vamsi K Komarala** (DESE), **Dr. Sandeep Pathak** (DESE), **Dr. Vipin Kumar** (DESE), and **Dr. Samaresh Das** (CARE) for their constant help and advice. I also thank all the faculty members of DESE and the administrative staff for their valuable support.

My sincere regards to Nanoscale Research Facility (NRF) and Central Research Facility's (CRF) faculty members and TAs for their support during characterization. I am also thankful to the **Ministry of Education** formerly known as the **Ministry of Human Resource Development** for their financial support.

I thank my fellow lab mates of the Organic and Hybrid Electronic Device Laboratory (OHEDL), along with all members of the PV group for providing their support. The journey was not that much beautiful without my friends. I owe a deep sense of gratitude to my friends who supported me in hard times and celebrated each accomplishment: **Dr. Mandakini Sharma, Dr. Sobia Waheed**. Their cooperation would be an unforgettable experience.

An endeavour on the long journey of a Ph.D. requires sacrifice not only on the part of the student but also from his close family members. I will never be able to repay the efforts laid down by my parents to prepare me for this study. My parents deserve special attention for their everlasting support, love, prayers, care, and sacrifice. My loving parents **Mrs. Madhu Pareek** and **Mr. Rajendra Kumar Pareek** are in the first place who rooted the strength in my character, showing me the joy of intellectual pursuit since childhood. It is their love, sacrifice, and support through the years that landed me at the Indian Institute of Technology Delhi (IIT Delhi) and provided the strength for the completion of my Ph.D. thesis. I can never thank you enough **Mummy** and **Papa**.

The words and ideas that follow represent only a small share of everything that happened in the completion of this thesis. It is the success that you read in these pages; however, the undocumented failures and minor successes also make up this thesis. It is due to the group of people described above, that all of this was possible. During My time at IIT Delhi, I made scientific, and personal discoveries, published articles, got the opportunity to travel abroad, and developed lifelong friendships.

Before, I finish I offer my regards and blessings to all those who supported me and offered me their gracious help in any aspect of the completion of this research work, with my sincere apology, if I was not able to mention all of them individually.

Saurabh Pareek

Abstract

Graphitic carbon nitride is a 2-dimensional material analogous to graphite. It possesses a layered structure consisting of triazine or heptazine motifs arranged in a hexagonal fashion. Owing to its layered structure, bonded via weak Van der Waals forces, it can delaminate the bulk material into graphene-like novel nanostructures (nanosheets and quantum dots). It possesses promising material properties such as n-type semiconducting nature, strong absorption in UV-visible region, high chemical stability, and tunable optoelectronic properties making it a potential candidate for optoelectronic device applications. Herein, we have demonstrated the facile synthesis strategy to synthesize g-C₃N₄ nanosheets (NS) and quantum dots (QDs) by green route using water as the exfoliating agent and chemical acidification of bulk material followed by hydrothermal treatment, respectively. The structural and optical properties were investigated in detail to understand the structure-property relationship of prepared low-dimensional materials. It was observed that the chemical structure was well preserved even after exfoliation and acidification of bulk material into nanosheets and quantum dots. The NS and QDs possess an ultra-thin nature as evidenced by AFM and HRTEM images having thicknesses below 5 nm and 1.7 nm, respectively. These nanostructures possess tunability in optical properties as observed from blue-shifted absorption and emission spectra. Moreover, a reduction in Urbach energy after exfoliation suggests a smaller probability of photogenerated carrier recombination. These appealing properties pave the path for the utilization of these nanostructures for photovoltaic applications either as an additive for the active/interface layer or as a charge-selective interface layer.

The multi-functionality of the prepared quantum dots was explored as an additive for poly(3-hexylthiophene-2,5-diyl):[6,6]-phenyl-C71-butyric acid methyl ester (P3HT:PC₇₁BM) blend active layer. The QDs were prepared in an organic solvent (o-dichlorobenzene) to maintain compatibility with the device fabrication process. The photovoltaic effect formation

and various effects of g-C₃N₄ QDs on energy transfer, carrier transport, and nanoscale morphology were investigated in detail by incorporation as a third component into a well-established material combination of P3HT:PC₇₁BM blend films. The emission spectra of g-C₃N₄ QDs and absorption spectra of P3HT were found to have overlapping features that enabled the QDs to transfer ultraviolet region photons to P3HT. The g-C₃N₄ QDs were found to assist Förster resonance energy transfer (FRET) between the QDs and host polymer, improving the overall energy harvesting capability of the devices. Moreover, g-C₃N₄ QDs were favorable in maintaining nanoscale phase segregation of the active layer with improved crystallinity which is crucial for efficient exciton dissociation and faster charge extraction. The incorporation of g-C₃N₄ QDs, improved the device efficiency by almost 40% for optimal concentration of QDs i.e., 2 Vol% compared to reference one. The improved device efficiency is thus attributed to the combined consequences of improved morphology and the FRET effect.

The g-C₃N₄ NS and QDs were utilized as a secondary dopant to modulate the structural and electronic properties of commonly used hole transport layer viz. PEDOT:PSS. The addition of NS and QDs weakened the columbic interaction between the PEDOT and PSS leading to the formation of an expanded coil-like structure. This resulted in the reorientation of the PEDOT chain forming the interconnected charge transport pathways thereby, improving the conductivity of modified films. When employed as a hole transport layer in polymer solar cells they yielded the power conversion efficiency of 7.65% and 6.44% at an optimal concentration of 50 Vol% and 60 Vol% for NS and QDs, respectively, compared to 5.45% for reference one. This improvement in photovoltaic performance can be attributed to the increased short circuit current density (J_{SC}), charge carrier mobility, fill factor (FF), and reduced series resistance (R_s). However, the FF was higher for NS-based devices as they provide better continuous charge hopping pathways compared to QDs. Moreover, the modification in the molecular structure of PEDOT:PSS via NS and QDs resulted in improved device stability compared to reference one,

retaining almost 40% of initial power conversion efficiency even after 200 min of continuous illumination. These results demonstrate the systematic strategy for improving the conductivity and mobility of HTL resulting in efficient extraction of charge carriers, enhanced device performance, and stability.

The g-C₃N₄ NS was utilized as a charge-selective interface layer in polymer solar cells both for extraction of electrons and holes. The work function of ITO decreased from 4.94 eV to 4.43 eV after coating with NS. However, with UV-ozone (UV-O₃) treatment gradual increase in work function was observed and for the optimal treatment duration (10 min), it reaches 5.25 eV. This suggests that in its pristine form, i.e., untreated ITO/g-C₃N₄ NS, it can extract electrons and therefore can be utilized as the cathode interface layer for inverted solar cells while after UV-O₃ treatment it facilitates the extraction of holes and thereby can be used as an anode interface layer in conventional device architecture. This has been demonstrated with the active layer combination of PTB7-Th:PC₇₁BM. Similar short circuit current densities (15.65 mA cm⁻²) and power conversion efficiencies (5.60% and 6.05%) were observed for both inverted and conventional devices having g-C₃N₄ NS as the charge selective interface layer. The UV-O₃ treatment seems to modify the g-C₃N₄ NS thin film by inducing surface dipoles due to the incorporation of oxygen atoms which is primarily responsible for their switching behavior of work function as observed. This study demonstrates the dual functionality of g-C₃N₄ NS as a charge-selective interface layer (CIL/AIL) for solution-processable polymer solar cells.

The g-C₃N₄ possesses unique optoelectronic properties, however, its thin-film characteristics were not well explored, therefore, limiting its utilization for semiconductor device applications. Herein, we fabricated the thin film of 10 nm via thermal evaporation and studied the effect of UV-O₃ treatment on structural, optical, electrical, and dielectric properties. Systematic improvements in film characteristics were observed until 10 min treatment

duration. However, a further increase in treatment duration resulted in a detrimental effect on the thin-film properties. It was observed that the structure was well retained for the thin film after thermal evaporation and UV-O₃ treatment, as that of bulk g-C₃N₄. Moreover, the thermally evaporated film exhibited a smooth surface with r.m.s roughness well below 1 nm and the smoothness of the film further increased after treatment. The emission properties and Urbach energy analysis suggested reduced charge carrier recombination leading to better photo-induced charge separation in thin film after UV-O₃ treatment. The treated thin film exhibited a smaller leakage current resulting in a higher dielectric constant and smaller loss.

All the above results suggest that g-C₃N₄ nanostructures and thin film possess appealing structural, optical, and electrical properties which can significantly improve the performance of polymer solar cells. However, its several unique features pave the path towards utilization in other semiconductor devices too, like perovskite solar cells, light emitting diodes, photodetectors, wearable technology devices, energy storage devices etc.

सारांश

ग्राफिटिक कार्बन नाइट्राइड ग्रेफाइट के अनुरूप एक 2-आयामी सामग्री है। इसमें एक स्तरित संरचना होती है जिसमें एक हेक्सागोनल फैशन में व्यवस्थित ट्राइज़िन या हेप्टाज़िन रूपांकनों से मिलकर बनता है। कमजोर वेंडर वाल्स बलों के माध्यम से बंधे इसकी स्तरित संरचना के कारण, यह थोक सामग्री को ग्राफीन जैसे नए नैनोस्ट्रक्चर (नैनोशीट्स और क्वांटम डॉट्स) में बदल सकता है। इसमें एन-टाइप सेमीकंडक्टिंग प्रकृति, यूवी-दृश्य क्षेत्र में मजबूत अवशोषण, उच्च रासायनिक स्थिरता और ट्यून करने योग्य ऑप्टोइलेक्ट्रॉनिक गुण जैसे आशाजनक भौतिक गुण हैं, जो इसे ऑप्टोइलेक्ट्रॉनिक डिवाइस अनुप्रयोगों के लिए एक संभावित उम्मीदवार बनाते हैं। इसमें हमने $g\text{-C}_3\text{N}_4$ नैनोशीट्स (NS) और क्वांटम डॉट्स (QDs) को हरित मार्ग से संश्लेषित करने के लिए सरल संश्लेषण रणनीति का प्रदर्शन किया है, जिसमें क्रमशः पानी को एक्सफोलिएटिंग एजेंट के रूप में उपयोग किया जाता है और हाइड्रोथर्मल उपचार के बाद थोक सामग्री का रासायनिक अम्लीकरण किया जाता है। तैयार निम्न-आयामी सामग्रियों की संरचना-संपत्ति संबंध को समझने के लिए संरचनात्मक और ऑप्टिकल गुणों की विस्तार से जांच की गई। यह देखा गया कि नैनोशीट्स और क्वांटम डॉट्स में थोक सामग्री के एक्सफोलिएशन और अम्लीकरण के बाद भी रासायनिक संरचना अच्छी तरह से संरक्षित थी। NS और QDs में एक अल्ट्रा-पतली प्रकृति होती है, जैसा कि AFM और HRTEM छवियों द्वारा क्रमशः 5 nm और 1.7 nm से कम मोटाई होती है। इन नैनोस्ट्रक्चर में ऑप्टिकल गुणों में ट्यूनेबिलिटी होती है जैसा कि ब्लू शिफ्टेड अवशोषण और उत्सर्जन स्पेक्ट्रा से देखा जाता है। इसके अलावा, एक्सफोलिएशन के बाद उर्बाक ऊर्जा में कमी फोटोजेनरेटेड वाहक पुनर्संयोजन की एक छोटी संभावना का सुझाव देती है। ये आकर्षक गुण फोटोवोल्टिक अनुप्रयोगों के लिए इन नैनोस्ट्रक्चर के उपयोग के लिए मार्ग प्रशस्त करते हैं या तो सक्रिय/इंटरफ़ेस परत के लिए एक योजक के रूप में या चार्ज चयनात्मक इंटरफ़ेस परत के रूप में।

तैयार क्वांटम डॉट्स की बहु-कार्यक्षमता को पॉली (3-हेक्सिलथियोफीन -2,5-डाइल):[6,6]-फिनाइल-सी-71-ब्यूटिरिक एसिड मिथाइल एस्टर (P3HT:PC₇₁BM) मिश्रण सक्रिय परत के लिए एक

योजक के रूप में खोजा गया था। डिवाइस निर्माण प्रक्रिया के साथ संगतता बनाए रखने के लिए QDs को कार्बनिक विलायक (ओ-डाइक्लोरोबेंजीन) में तैयार किया गया था। फोटोवोल्टिक प्रभाव गठन और ऊर्जा हस्तांतरण, वाहक परिवहन और नैनोस्केल आकृति विज्ञान पर $g-C_3N_4$ QDs के विभिन्न प्रभावों की P3HT:PC₇₁BM मिश्रण फिल्मों के एक अच्छी तरह से स्थापित सामग्री संयोजन में तीसरे घटक के रूप में शामिल करके विस्तार से जांच की गई थी। $g-C_3N_4$ QDs के उत्सर्जन स्पेक्ट्रा और P3HT के अवशोषण स्पेक्ट्रा में अतिव्यापी विशेषताएं पाई गईं जो QDs को पराबैंगनी क्षेत्र फोटॉन को P3HT में स्थानांतरित करने में सक्षम बनाती हैं। $g-C_3N_4$ QDs को QDs और होस्ट पॉलीमर के बीच फोरस्टर अनुनाद ऊर्जा हस्तांतरण (FRET) की सहायता करने के लिए पाया गया, जिससे उपकरणों की समग्र ऊर्जा संचयन क्षमता में सुधार हुआ। इसके अलावा, $g-C_3N_4$ QDs बेहतर स्फटिकता के साथ सक्रिय परत के नैनोस्केल चरण अलगाव को बनाए रखने में अनुकूल थे जो कुशल एक्सीटोनिक पृथक्करण और तेजी से चार्ज निष्कर्षण के लिए महत्वपूर्ण है। $g-C_3N_4$ QDs के समावेश ने QDs की इष्टतम सांद्रता के लिए डिवाइस दक्षता में लगभग 40% का सुधार किया, यानी संदर्भ की तुलना में 2 Vol%। इस प्रकार बेहतर उपकरण दक्षता को बेहतर आकृति विज्ञान और FRET प्रभाव के संयुक्त परिणामों के लिए जिम्मेदार ठहराया जाता है।

$g-C_3N_4$ NS और QDs का उपयोग आमतौर पर उपयोग किए जाने वाले होल परिवहन परत viz. PEDOT:PSS के संरचनात्मक और इलेक्ट्रॉनिक गुणों को संशोधित करने के लिए द्वितीयक डोपेंट के रूप में किया गया था। NS और QDs के प्रयोग से PEDOT और PSS के बीच कोलम्बिक इंटरैक्शन कमजोर हो गया, जिससे एक विस्तारित कॉइल जैसी संरचना का निर्माण हुआ। इसके परिणामस्वरूप PEDOT श्रृंखला का पुनर्विन्यास हुआ, जिससे परस्पर चार्ज परिवहन मार्गों का निर्माण हुआ, जिससे संशोधित फिल्मों की चालकता में सुधार हुआ। जब पॉलीमर सोलर सेल में होल परिवहन परत के रूप में नियोजित किये जाने पर उन्होंने NS और QDs के लिए क्रमशः 50 Vol% और 60 Vol% की इष्टतम सांद्रता पर 7.65% और 6.44% की बिजली रूपांतरण दक्षता प्राप्त की, जबकि संदर्भ के लिए यह 5.45%

थी। फोटोवोल्टिक प्रदर्शन में इस सुधार को शॉर्ट सर्किट करंट घनत्व (J_{sc}), चार्ज वाहक गतिशीलता, फिल फैक्टर (FF), और कम श्रृंखला प्रतिरोध (R_s) के लिए जिम्मेदार ठहराया जा सकता है। हालांकि, NS-आधारित उपकरणों के लिए FF अधिक था क्योंकि वे QDs की तुलना में बेहतर निरंतर चार्ज होपिंग मार्ग प्रदान करते हैं। इसके अलावा, NS और QDs के माध्यम से PEDOT:PSS की आणविक संरचना में संशोधन के परिणामस्वरूप संदर्भ की तुलना में डिवाइस स्थिरता में सुधार हुआ, 200 मिनट की निरंतर रोशनी के बाद भी प्रारंभिक बिजली रूपांतरण दक्षता का लगभग 40% तक बरकरार रहा। ये परिणाम HTL की चालकता और गतिशीलता में सुधार के लिए व्यवस्थित रणनीति का प्रदर्शन करते हैं जिसके परिणामस्वरूप चार्ज वाहक का कुशल निष्कर्षण, डिवाइस प्रदर्शन और स्थिरता बढ़ी है।

$g-C_3N_4$ NS का उपयोग इलेक्ट्रॉन और होल के निष्कर्षण के लिए पॉलीमर सोलर सेल में चार्ज-चयनात्मक इंटरफ़ेस परत के रूप में किया गया था । NS की कोटिंग के बाद आईटीओ का कार्य-फलन 4.94 eV से घटकर 4.43 eV हो गया। हालांकि, यूवी-ओज़ोन (UV- O_3) उपचार के साथ कार्य-फलन में क्रमिक वृद्धि देखी गई और इष्टतम उपचार अवधि (10 min) के लिए, यह 5.25 eV तक पहुंच जाता है । इससे पता चलता है कि अपने प्राचीन रूप में, यानी अनुपचारित ITO/ $g-C_3N_4$ NS, यह इलेक्ट्रॉनों को निकाल सकता है और इसलिए इनवर्टेड पॉलीमर सोलर सेल के लिए कैथोड इंटरफ़ेस परत के रूप में उपयोग किया जा सकता है, जबकि UV- O_3 उपचार के बाद यह होल के निष्कर्षण की सुविधा प्रदान करता है और इस तरह इसका उपयोग कन्वेंशनल डिवाइस आर्किटेक्चर में एनोड इंटरफ़ेस परत के रूप में किया जा सकता है। यह PTB7-Th:PC₇₁BM के सक्रिय परत संयोजन के साथ प्रदर्शित किया गया है। चार्ज सेलेक्टिव इंटरफ़ेस लेयर के रूप में $g-C_3N_4$ NS वाले इनवर्टेड और कन्वेंशनल दोनों डिवाइस के लिए समान शॉर्ट सर्किट करंट घनत्व (15.65 mA cm⁻²) और पावर रूपांतरण क्षमता (5.60% और 6.05%) देखी गई है। UV- O_3 उपचार ऑक्सीजन परमाणुओं के समावेश के कारण सतह द्विध्रुवीय को प्रेरित करके $g-C_3N_4$ NS पतली परत को संशोधित करता है जो मुख्य रूप से कार्य-फलन के उनके स्विचिंग व्यवहार के लिए जिम्मेदार है। यह अध्ययन समाधान-संसाधित पॉलीमर सोलर सेल के लिए

चार्ज-चयनात्मक इंटरफ़ेस परत (CIL/AIL) के रूप में $g-C_3N_4$ NS की दोहरीकार्यात्मकता को प्रदर्शित करता है।

$g-C_3N_4$ में अद्वितीय ऑटोइलेक्ट्रॉनिक गुण हैं, हालांकि, इसकी पतली-परत कि विशेषताओं को अच्छी तरह से खोजा नहीं गया था, इसलिए, अर्धचालक उपकरण अनुप्रयोगों के लिए इसका उपयोग सीमित रह गया है। यहां, हमने थर्मल वाष्पीकरण के माध्यम से 10 nm की पतली परत बनाई और संरचनात्मक, ऑप्टिकल, विद्युत और परावैद्युत गुणों पर UV- O_3 उपचार के प्रभाव का अध्ययन किया। फिल्म विशेषताओं में व्यवस्थित सुधार 10 मिनट की उपचार अवधि तक देखा गया था। हालांकि, उपचार की अवधि में और वृद्धि के परिणामस्वरूप पतली-परत के गुणों पर हानिकारक प्रभाव पड़ा। यह देखा गया कि थर्मल वाष्पीकरण और UV- O_3 उपचार के बाद पतली परत के लिए संरचना को अच्छी तरह से बरकरार रखा गया था, जैसा कि थोक $g-C_3N_4$ की है। इसके अलावा, थर्मल रूप से वाष्पित परत में 1 nm से नीचे r.m.s खुरदरापन के साथ एक स्मूथ सतह का प्रदर्शन किया और उपचार के बाद फिल्म की स्मूथनेस और बढ़ गई। उत्सर्जन गुणों और उरबैक ऊर्जा विश्लेषण ने कम चार्ज वाहक पुनर्संयोजन का सुझाव दिया, जिससे UV- O_3 उपचार के बाद पतली परत में बेहतर फोटो-प्रेरित चार्ज पृथक्करण हुआ। उपचारित पतली परत ने एक कम करंट के रिसाव का प्रदर्शन किया जिसके परिणामस्वरूप एक उच्च परावैद्युत स्थिरांक और छोटा नुकसान हुआ।

उपरोक्त सभी परिणाम बताते हैं कि $g-C_3N_4$ नैनोस्ट्रक्चर और पतली परत में आकर्षक संरचनात्मक, ऑप्टिकल और विद्युत गुण होते हैं जो पॉलीमर सोलर सेल के प्रदर्शन में काफी सुधार कर सकते हैं। हालांकि, इसकी कई अनूठी विशेषताएं अन्य अर्धचालक उपकरणों में भी उपयोग की दिशा में मार्ग प्रशस्त करती हैं, जैसे पेरोवस्काइट सोलर सेल, प्रकाश उत्सर्जक डायोड, फोटोडिटेक्टर, वियरेबल टेक्नॉलॉजी उपकरण, ऊर्जा भंडारण उपकरण आदि।

Table of Contents

CERTIFICATE.....	i
Acknowledgments	ii
Abstract.....	iv
सारांश.....	viii
Table of Contents	xii
List of Figures.....	xvii
List of Tables	xxiv
Abbreviations and Symbols	xxv
Chapter 1: Introduction	2
1.1 Background.....	2
1.2 Sun Energy and Solar Spectrum	4
1.3 Solar Cell Technologies.....	7
1.4 Organic Photovoltaic	10
1.4.1 Working Principle.....	11
1.4.2 Device Architecture	14
1.5 Solar Cell Characteristics.....	17
1.6 Introduction to Graphitic carbon nitride (g-C ₃ N ₄).....	20
1.6.2 Properties of graphitic carbon nitride	27
1.6.3 Graphitic carbon nitride for optoelectronic applications	31

1.7 Objectives	33
1.8 Thesis Organization	34
References.....	36
Chapter 2: Structural and optical properties of graphene like carbon nitride into nanosheets and quantum dots.....	62
2.1 Introduction.....	62
2.2 Experimental Section.....	64
2.2.1 Materials	64
2.2.2 Synthesis of graphitic carbon nitride (g-C ₃ N ₄).....	64
2.2.3 Synthesis of g-C ₃ N ₄ nanosheets.....	64
2.2.4 Synthesis of g-C ₃ N ₄ Quantum Dots.....	64
2.3 Material Characterization.....	65
2.4 Results and Discussion	65
2.5 Conclusion	74
References.....	76
Chapter 3: Graphitic carbon nitride quantum dots (g-C₃N₄ QDs) to improve photovoltaic performance of polymer solar cell by combining förster resonance energy transfer (FRET) and morphological effects	84
3.1 Introduction.....	84
3.2 Experimental Section.....	86
3.2.1 Materials	86
3.2.2 Synthesis of graphitic carbon nitride quantum dots (g-C ₃ N ₄ QDs).....	86

3.3 Device Fabrication	86
3.4 Material Characterization.....	87
3.5 Results and Discussion	88
3.5.1 Characterization of g-C ₃ N ₄ QDs.....	88
3.5.2 Effect of QDs on the morphology of P3HT: PC ₇₁ BM blend active layer	91
3.5.3 Effect of QDs on optical properties of the film	93
3.5.4 Photovoltaic Performance of devices.....	96
3.6 Conclusion	100
References.....	101
Chapter 4: Graphitic carbon nitride nanostructures as molecular modifier for PEDOT:PSS hole transport layer in polymer solar cells	111
4.1 Introduction.....	111
4.2 Experimental Section	113
4.2.1 Materials	113
4.2.2 Synthesis of graphitic carbon nitride (g-C ₃ N ₄) and its nanostructures	113
4.2.3 Preparation of Hole transport layers (HTLs)	114
4.3 Device Fabrication	114
4.4 Measurement and Characterization.....	114
4.5 Results and Discussion	115
4.5.1 Characterization of g-C ₃ N ₄ nanostructures.....	115
4.5.2 Photovoltaic characteristics with different HTLs	116

4.5.3 Opto-electronic and structural properties of the nanostructure modified PEDOT:PSS film.....	123
4.5.4 Mobility measurement and charge carrier dynamics	128
4.6 Conclusion	130
References.....	131
Chapter 5: Dual functional graphitic carbon nitride nanosheets as charge selective cathode/anode interface layer for polymer solar cells	139
5.1 Introduction.....	139
5.2 Experimental Section	140
5.2.1 Materials	140
5.2.2 Synthesis of graphitic carbon nitride nanosheets.....	140
5.3 Device Fabrication	141
5.4 Measurement and Characterization.....	141
5.5 Results and Discussion	142
5.5.1 Structural and optical properties of g-C ₃ N ₄ NS	142
5.5.2 Work function measurement of g-C ₃ N ₄ NS thin film.....	143
5.5.3 Photovoltaic characteristics	146
5.5.3.1 Inverted device.....	147
5.5.3.2 Conventional device.....	149
5.6 Conclusion	153
References.....	154

Chapter 6: The effect of UV-ozone treatment on structural, optical, and dielectric properties of thermally evaporated graphitic carbon nitride thin film	159
6.1 Introduction.....	159
6.2 Experimental Section	160
6.2.1 Materials	160
6.2.2 Synthesis of bulk graphitic carbon nitride	160
6.2.3 Preparation of g-C ₃ N ₄ thin film	160
6.2.4 Deposition of Aluminium (Al) electrode	161
6.3 Measurement and Characterization.....	161
6.4 Results and Discussion	161
6.4.1 Structural properties of g-C ₃ N ₄ thin film.....	161
6.4.2 Optoelectronic characteristics of g-C ₃ N ₄ thin film.....	163
6.4.3 Electrical and Dielectric properties of g-C ₃ N ₄ thin film.....	167
6.5 Conclusion	170
References.....	171
Chapter 7: Conclusions and Future Scope	177
7.1 Summary.....	177
7.2 Future Scope	178
Appendix A	180
Appendix B	184
LIST OF PUBLICATIONS	188
About the Author	192

List of Figures

Chapter 1

- Fig. 1.1** Worldwide per capita energy consumption in 2021 (Image Source: OurWorldIndata.org/energy)3
- Fig. 1.2** Spectral distribution of sunlight reaching the outside the earth’s atmosphere, the blue curve shows the extra-terrestrial radiation and red one depicts the black body radiation modelled using plank’s law. (Image credit: <https://eclipse2017.nasa.gov/what-color-sun>).4
- Fig. 1.3** Interaction of sun radiation with the earth’s atmosphere5
- Fig. 1.4** Definition of different Air Mass (AM) conditions (Image source: <https://www.laserfocusworld.com/lasers-sources/article/16566681/photovoltaics-measuring-the-sun>)6
- Fig. 1.5** The chart for best power conversion efficiency, measured under standard testing conditions, for various photovoltaic technologies, maintained by National Renewable Energy Laboratory (NREL). (This plot is courtesy of the NREL, Golden, CO.)8
- Fig. 1.6** Working mechanism of Organic Solar cells (a) light absorption and exciton generation, (b) exciton diffusion, (c) exciton dissociation, (d) charge transport, (e) charge collection. ...13
- Fig. 1.7** (a) Schematic illustration of single layer OPV device, (b) corresponding energy band diagram.15
- Fig. 1.8** (a) Schematic illustration of bi-layer OPV device, (b) corresponding energy band diagram.15
- Fig. 1.9** Schematic illustration of (a) bulk heterojunction, (b) ordered heterojunction based OPV device, (c) corresponding energy band diagram.16
- Fig. 1.10** (a) Current Density vs voltage (J-V) characteristic of the solar cell, (b) equivalent circuit for modelling the J-V characteristic.18

Fig. 1.11 J-V characteristics of solar cell depicting the effect of parasitic resistances (R_s and R_{sh}) on fill factor of device.	19
Fig. 1.12 Various types of $g-C_3N_4$ depending on micro/nano structures and morphologies...	22
Fig. 1.13 structural models of graphitic carbon nitride based on (I) triazine (II) tri-s-triazine motifs, and (III) model proposed by Lotsch et al. [192].	28

Chapter 2

Fig. 2.1 Schematic illustration of the synthesis of bulk $g-C_3N_4$, $g-C_3N_4$ nanosheets, and quantum dots.....	66
Fig. 2.2 (a) XRD pattern of bulk $g-C_3N_4$, $g-C_3N_4$ nanosheets, and quantum dots, (b) schematic illustration of (100) and (002) planes.....	67
Fig. 2.3 FTIR spectra of bulk $g-C_3N_4$, $g-C_3N_4$ nanosheets, and quantum dots.	68
Fig. 2.4 HRTEM images of (a) bulk $g-C_3N_4$, (b) $g-C_3N_4$ nanosheets, (c) quantum dots and (d) particle size distribution of QDs with Gaussian fit.....	69
Fig. 2.5 AFM images with a corresponding height profile of bulk $g-C_3N_4$ (a, d) , $g-C_3N_4$ nanosheets (b, e) , and quantum dots (c, f)	70
Fig. 2.6 (a) UV-vis absorption spectra with tauc plot in the inset (b) urbach energy plot of bulk $g-C_3N_4$, $g-C_3N_4$ nanosheets, and quantum dots.	71
Fig. 2.7 (a) Photoluminescence (PL) spectra of bulk $g-C_3N_4$, $g-C_3N_4$ nanosheets, and quantum dots, (b) UV-vis absorption and PL spectra of bulk $g-C_3N_4$ and quantum dots (stokes shift). The inset of (b) shows the digital image of an aqueous solution of QDs under UV light, UV-vis, and PL spectra of $g-C_3N_4$ nanosheets.....	72
Fig. 2.8 Schematic illustration of energy level diagram for PL emission from the $g-C_3N_4$	73

Chapter 3

Fig. 3.1 X-Ray Diffraction pattern of bulk $g-C_3N_4$ and $g-C_3N_4$ QDs.....	88
--	----

Fig. 3.2 HRTEM images (a) bulk g-C ₃ N ₄ , (b) g-C ₃ N ₄ QDs, (c) HRTEM Fringes of g-C ₃ N ₄ QDs, and (d) Particle size distribution of g-C ₃ N ₄ QDs with Gaussian fit	89
Fig. 3.3 FTIR spectra of bulk g-C ₃ N ₄ and g-C ₃ N ₄ QDs.	90
Fig. 3.4 (a) X-Ray Diffraction pattern for P3HT:PC ₇₁ BM film for different concentrations of g-C ₃ N ₄ QDs, (b) crystallite size variation with QDs concentration.	91
Fig. 3.5 AFM images (a) P3HT:PC ₇₁ BM, (b-e) 2 Vol%, 4 Vol%, 6 Vol%, and 8 Vol% of g-C ₃ N ₄ QDs concentration and (f) roughness estimation.....	92
Fig. 3.6 (a) Optical characteristics of g-C ₃ N ₄ QDs, P3HT, (b) photoluminescence spectra of P3HT and their mixture with different concentrations of g-C ₃ N ₄ QDs.	93
Fig. 3.7 (a) UV-vis absorption spectra of P3HT:PC ₇₁ BM with different concentrations of g-C ₃ N ₄ QDs, (b) frenkel exciton bandwidth versus g-C ₃ N ₄ QDs concentration.	94
Fig. 3.8 Photoluminescence spectra of P3HT and P3HT:PC ₇₁ BM with different concentrations of g-C ₃ N ₄ QDs.	96
Fig. 3.9 (a) Current density vs voltage (J-V) characteristic of P3HT:PC ₇₁ BM with different concentrations of g-C ₃ N ₄ QDs, (b) Photovoltaic parameter variations.	97
Fig. 3.10 Dark J-V characteristic of P3HT:PC ₇₁ BM with different concentrations of g-C ₃ N ₄ QDs.	98
Fig. 3.11 Current density vs voltage (J-V) curve of (a) electron-only device, (b) hole-only device, (c) mobility variation of P3HT:PC ₇₁ BM with different concentrations of g-C ₃ N ₄ QDs.	99

Chapter 4

Fig. 4.1 (a) Absorbance (b) FTIR spectra of bulk g-C ₃ N ₄ , g-C ₃ N ₄ nanosheets, and quantum dots, HRTEM images of (c) g-C ₃ N ₄ nanosheets and (d) quantum dots with particle size distribution in the inset.....	116
---	-----

Fig. 4.2 (a) Molecular structures of PEDOT, PSS, g-C ₃ N ₄ , PTB7-Th, PC ₇₁ BM and (b) schematic device architecture of polymer solar cell.	117
Fig. 4.3 UV-vis transmittance spectra of (a) NS and (b) QDs modified PEDOT:PSS HTLs with different concentrations.	117
Fig. 4.4 Current density vs voltage (J-V) characteristics of PTB7-Th:PC ₇₁ BM with different concentrations of (a) NS and (b) QDs modified PEDOT:PSS HTL.	118
Fig. 4.5 (a) Current density vs voltage (J-V) characteristics and (b) external quantum efficiency with integrated J _{sc} of PTB7-Th:PC ₇₁ BM devices with different HTLs.	120
Fig. 4.6 (a) Current density vs voltage (J-V) characteristics under dark and (b) photocurrent versus effective voltage characteristics of PTB7-Th:PC ₇₁ BM devices with different HTLs.	121
Fig. 4.7 Evolution of power conversion efficiency normalized to their initial values (at t = 0 min) under continuous illumination.	122
Fig. 4.8 (a) Schematic illustration for conductivity measurement and (b) I-V characteristics of pristine and NS/QDs modified PEDOT:PSS thin film.	124
Fig. 4.9 (a) Raman spectra for pristine and NS/QDs modified thin films and (b) schematic illustration of conformational structure of PEDOT:PSS.	126
Fig. 4.10 AFM image for different HTLs (a) pristine PEDOT:PSS, (b) NS, and (c) QDs modified PEDOT:PSS.	127
Fig. 4.11 AFM image for PTB7-Th:PC ₇₁ BM active layer on different HTLs (a) pristine PEDOT:PSS, (b) NS, and (c) QDs modified PEDOT:PSS.	127
Fig. 4.12 Photoluminescence spectra of PTB7-Th and PTB7-Th:PC ₇₁ BM active layer on different HTL.	128
Fig. 4.13 (a) Current density vs voltage (J-V) characteristics for hole-only device and (b) Nyquist plot of PTB7-Th:PC ₇₁ BM with different HTLs. The inset of (b) shows the equivalent circuit used for fitting the curves.	129

Chapter 5

Fig. 5.1 (a) UV-vis absorbance, and (b) FTIR spectra of bulk g-C ₃ N ₄ and its nanosheets...	142
Fig. 5.2 HRTEM and AFM images of (a, c) bulk g-C ₃ N ₄ and (b, d) g-C ₃ N ₄ nanosheets. The inset of Fig. (c, d) shows the estimation of the number of layers.....	143
Fig. 5.3 Surface potential images with and w/o UV-O ₃ treatment measured from kelvin probe force microscope with estimated V _{CPD} values.	144
Fig. 5.4 Schematic illustration of inducing oxygen atoms on the surface of g-C ₃ N ₄ nanosheets thin film due to UV-O ₃ treatment.	145
Fig. 5.5 FTIR spectra of g-C ₃ N ₄ nanosheets thin film with and w/o UV-O ₃ treatment.	145
Fig. 5.6 UV-vis transmittance spectra of ITO and ITO/NS with and w/o UV-O ₃ treatment.	146
Fig. 5.7 Schematic illustration of (a) device configuration utilizing g-C ₃ N ₄ NS thin film as CIL, and (b) energy level diagram of inverted polymer solar cell.....	147
Fig. 5.8 (a) Current density vs voltage (J-V) characteristics, (b) external quantum efficiency, (c) dark J-V characteristics, and (d) photocurrent (J _{ph}) vs effective voltage characteristics of inverted device with and w/o g-C ₃ N ₄ NS thin film as cathode interface layer.....	148
Fig. 5.9 Schematic illustration of (a) device configuration utilizing g-C ₃ N ₄ NS thin film as AIL, and (b) energy level diagram of conventional polymer solar cell.	150
Fig. 5.10 (a) Current density vs voltage (J-V) characteristics of conventional device w/o and with UV-O ₃ treated g-C ₃ N ₄ NS thin film as anode interface layer, (b) photovoltaic parameter variations.....	151
Fig. 5.11 (a) Current density vs voltage (J-V) characteristics, (b) external quantum efficiency, (c) dark J-V characteristics, and (d) photocurrent (J _{ph}) vs effective voltage characteristics of the conventional device with and w/o UV-O ₃ treated g-C ₃ N ₄ NS thin film as an anode interface layer.....	152

Chapter 6

Fig. 6.1 FTIR spectra of g-C ₃ N ₄ thin film with and w/o UV-O ₃ treatment for the different time durations.....	162
Fig. 6.2 AFM images of g-C ₃ N ₄ thin film (a) w/o UV-O ₃ treatment, (b) 1 min, (c) 5 min, (d) 10 min, (e) 15 min, (f) 20 min of UV-O ₃ treatment duration, (g) roughness variation with UV-O ₃ treatment time.	163
Fig. 6.3 (a) UV-vis Absorbance spectra, inset shows the tauc plot, and (b) urbach energy plot of g-C ₃ N ₄ thin film with and w/o UV-O ₃ treatment.	164
Fig. 6.4 Steady-state photoluminescence spectra of g-C ₃ N ₄ thin film for different time duration of UV-O ₃ treatment at an excitation wavelength of 350 nm.	165
Fig. 6.5 Schematic illustration of electronic band transition for PL emission of g-C ₃ N ₄ thin films.	166
Fig. 6.6 Time-resolved photoluminescence spectra of g-C ₃ N ₄ thin film with and w/o UV-O ₃ treatment at a fixed emission wavelength of 425 nm.	167
Fig. 6.7 (a) Dark J-V characteristic and (b) corresponding double log-scale plot of g-C ₃ N ₄ thin film for the different time duration of UV-O ₃ treatment.	168
Fig. 6.8 (a) Dielectric constant and (b) dielectric loss of g-C ₃ N ₄ thin film with and w/o UV-O ₃ treatment.	169

Appendix A

Fig. A.1 Spectral overlap of emission spectra of g-C ₃ N ₄ QDs and absorption spectra of P3HT.	180
Fig. A.2 (a) Absorption spectra and (b) PL spectra of g-C ₃ N ₄ QDs at different concentrations.	181

Fig. A.3 Plot of area under PL curve vs. absorbance of g-C₃N₄ QDs at different concentrations.
..... 182

Fig. A.4 Schematic of the energy band diagram of materials used in polymer solar cell. 182

Appendix B

Fig. B.1 Cyclic voltammetry (C-V) curve of (a) pristine, (b) NS, (c) QDs modified PEDOT:PSS film coated over ITO, (d) peak oxidation current of different HTLs obtained from CV curve. 184

Fig. B.2 Raman spectra of pristine, NS/QDs modified PEDOT:PSS thin film..... 185

Fig. B.3 Current density vs voltage (J-V) characteristics of PTB7-Th:PC₇₁BM electron-only device. 186

List of Tables

Table 1.1 Solar irradiance at different Air Mass	7
Table 3.1 Photovoltaic parameters of the devices with different concentrations of g-C ₃ N ₄ QDs	97
Table 3.2 Electron and Hole mobility of P3HT:PC ₇₁ BM with different concentrations of g-C ₃ N ₄ QDs	99
Table 4.1 Photovoltaic parameters of PTB7-Th:PC ₇₁ BM devices with different concentrations of NS modified PEDOT:PSS HTL	118
Table 4.2 Photovoltaic parameters of PTB7-Th:PC ₇₁ BM devices with different concentrations of QDs modified PEDOT:PSS HTL	119
Table 5.1 Photovoltaic performance of PTB7-Th:PC ₇₁ BM device with and w/o anode interface layer.....	151
Table A1 Area of PL curve and absorbance value of g-C ₃ N ₄ QDs at different concentration	181
Table A2 FRET calculation from PHOTOCHEMCAD software.....	182
Table B1 Charge carrier mobility of PTB7-Th:PC ₇₁ BM devices	186

Abbreviations and Symbols

A	Acceptor
a-Si	Amorphous Silicon
AFM	Atomic Force Microscopy
Ag	Silver
Al	Aluminum
AM	Air Mass
CdTe	Cadmium Telluride
CdS	Cadmium Sulphide
CIGS	Copper Indium Gallium Selenide
CNT	Carbon Nanotube
D	Donor
DI	Deionized
DMF	Dimethyl formamide
DSSC	Dye Sensitized Solar cell
ETL	Electron Transport Layer
FF	Fill Factor
FTIR	Fourier Transform Infrared
g-C ₃ N ₄	Graphitic Carbon Nitride
GaAs	Gallium Arsenide
HOMO	Highest Occupied Molecular Orbit
HTL	Hole Transport Layer
IEA	International Energy Agency
IPA	Iso-Propyl Alcohol

IPCC	Intergovernmental Panel on Climate Change
kWh	kilo watt-hours
LUMO	Lowest Unoccupied Molecular Orbital
LiF	Lithium Fluoride
MTJ	Metric Tonne Joule
MPP	Maximum Power Point
NS	Nanosheets
NREL	National Renewable Energy Laboratory
OPV	Organic Photovoltaic
OSC	Organic Solar cell
P3HT	Poly(3-hexylthiophene)
PC ₇₁ BM	[6,6]-Phenyl-C71-butyric acid methyl ester
PCE	Power Conversion Efficiency
PHJ	Planar heterojunction
PL	Photoluminescence
PSC	Perovskite solar cell
PTFE	Polytetrafluoroethylene
PV	Photovoltaic
QDs	Quantum dots
r.m.s.	Root-mean-square
SAED	Selected Area Electron Diffraction
SEM	Scanning Electron Microscopy
SCLC	Space Charge Limited Current
Si	Silicon
TCO	Transparent Conducting Oxide

XRD	X-Ray Diffraction
q	Charge of electron
C	Capacitance
k_B	Boltzmann constant
ϵ_0	Free space permittivity
ϵ	Relative dielectric constant
μ	Mobility
η	Efficiency
eV	Electron volt
ml	Millilitre
μm	Micrometer
mA	Milliampere
meV	Milli electron volt
mg	Milligram
Nm	Nanometer
V_{bi}	Built-in-voltage
J_{max}	Current density at MPP
V_{max}	Voltage at MPP
J_{sc}	Short circuit current density
V_{oc}	Open circuit voltage
Z'	Real impedance (resistance)
Z''	Imaginary impedance (reactance)
τ	Time constant
Ω	Ohm